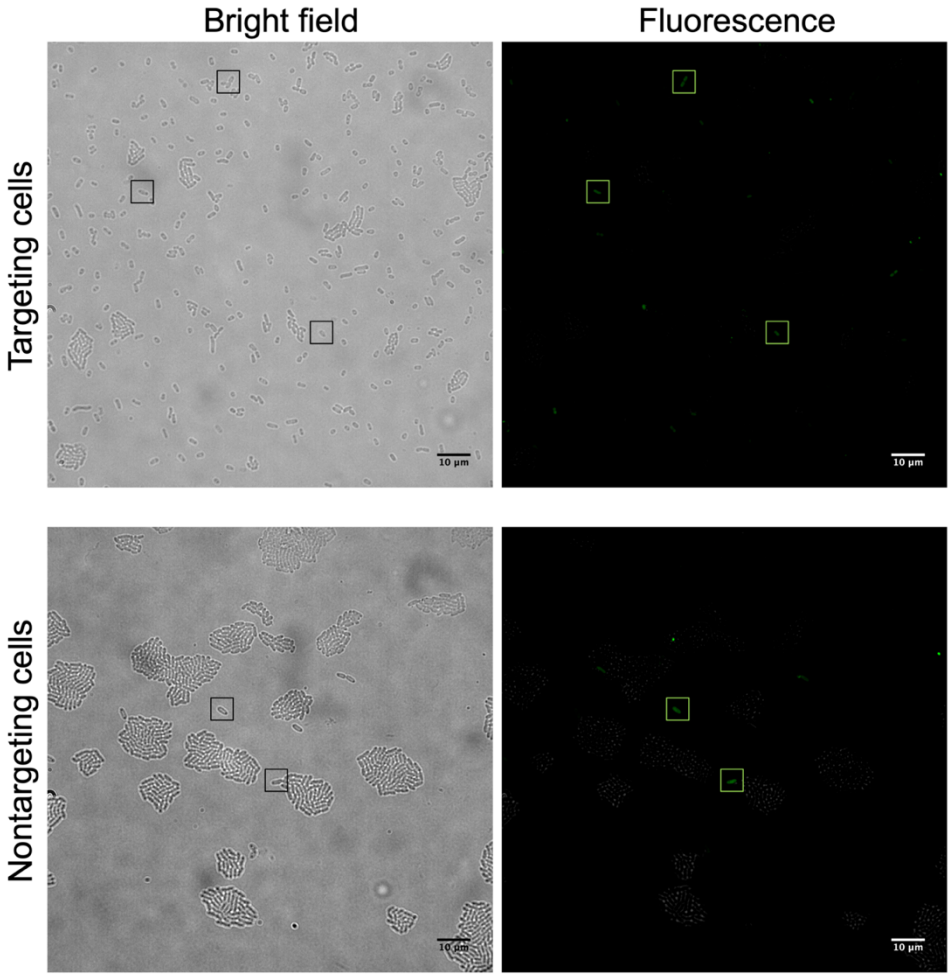

Fraction of dead cells, %

	Replica 1	Replica 2	Replica 3	Mean ± s. e. m.
Targeting cells	2.00	0.42	0	0.81 ± 0.61
Nontargeting cells	0.57	1.90	1.08	1.18 ± 0.39

Extended Data Fig. 1. YOYO-1 staining revealed a small number of dead cells equally in targeting and nontargeting cultures. Representative bright-field and fluorescence images of targeting and nontargeting cultures stained with a membrane-impermeable dye YOYO-1 for detection of dead cells. Bright-field and fluorescence images were acquired for the same field of view at 168 minutes post-induction. Small boxes indicate dead cells fluorescing green due to YOYO-1 bound to DNA. Statistics for dead cells' fraction was calculated from three biological replicates for targeting and nontargeting cultures. At least 100 cells were analyzed for each experiment.

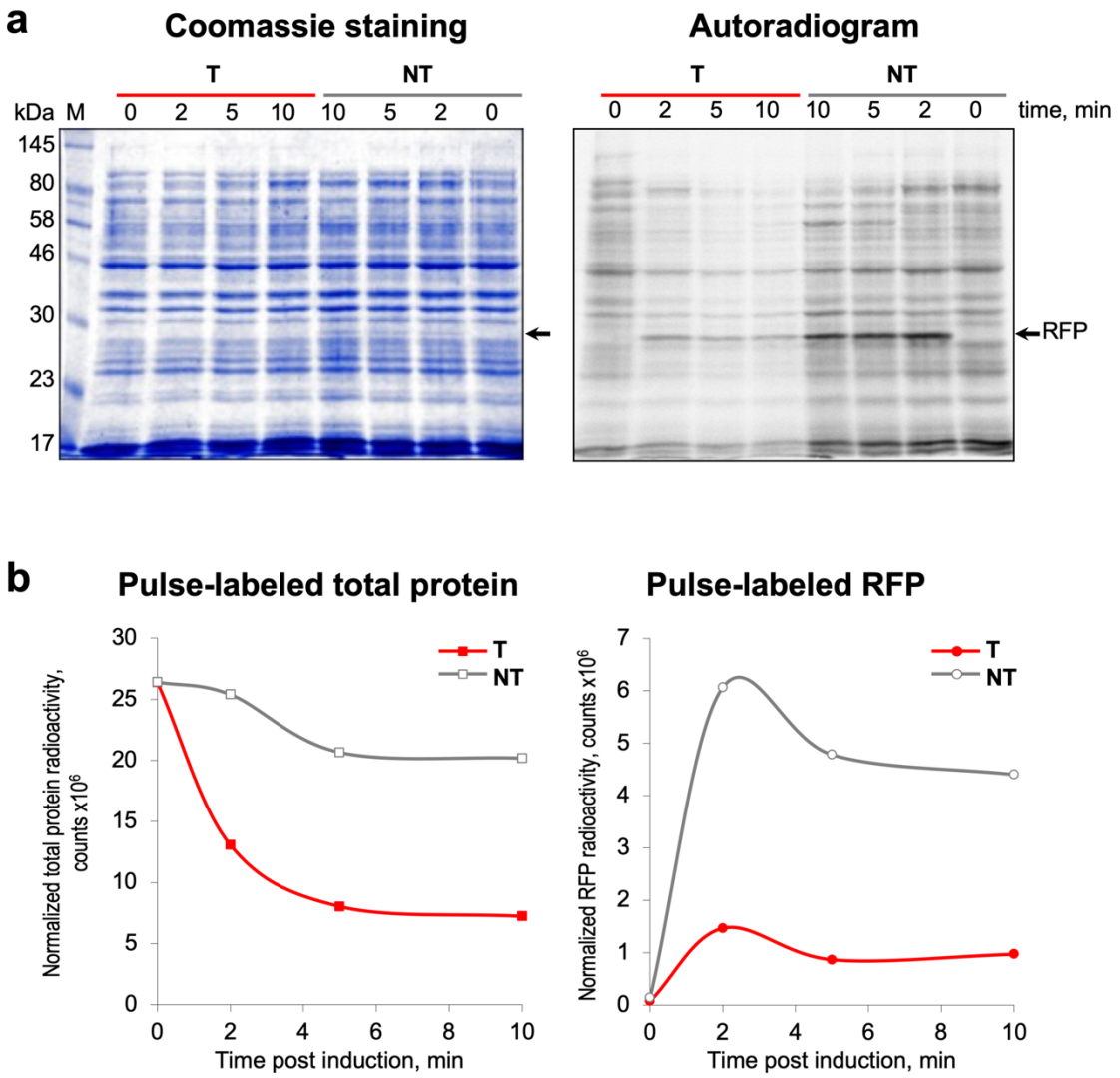

Extended Data Fig. 2. Time course of protein synthesis in targeting (T) and nontargeting (NT) cells after RFP induction. **a**, Protein samples obtained during pulse-labeling of *E. coli* cells by [^{35}S]-methionine, were separated by MOPS/SDS 10% PAGE, gels were stained by Coomassie, and quantified by Phosphorimager. The position of RFP on the gel and the autoradiogram is indicated by a black arrow. **b**, Graphs plots show the ^{35}S-radioactivity of pulse-labeled RFP and total cellular proteins in targeting (T, red) and nontargeting cells (NT, grey). For gel source data, see Supplementary Fig. 2.

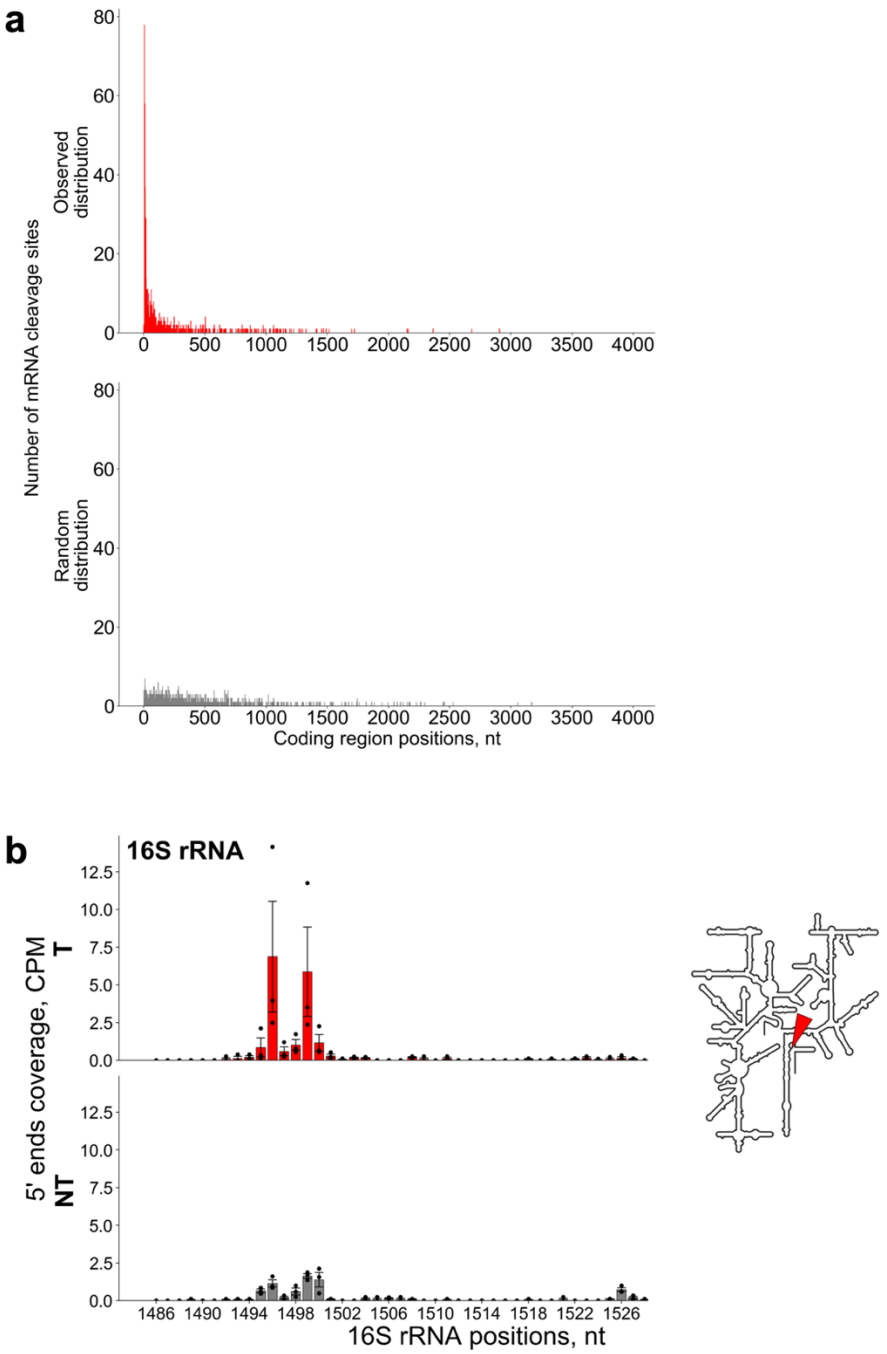

Extended Data Fig. 3. mRNA and 16SrRNA cleavages upon RFP mRNA targeting by Cas13a.

a, The distribution of top-1000 of mRNA cleavage sites (sorted by adjusted p-values in ascending order) across the positions of the coding regions revealed efficient cleavage at the beginning of coding sequences. **b**, 16S rRNA cleavage in targeting cells. Cut of 3'-end fragment containing anti-Shine-Dalgarno sequence or cleavage at this position in rRNA precursor. CPM normalized coverage of 5' ends of 16S rRNA in targeting (T, red bars) and nontargeting (NT, grey bars) samples of *E. coli* cells (mean ± s. e. m. from three biological replicates). The horizontal axis depicts the nucleotide position of 16S rRNA.

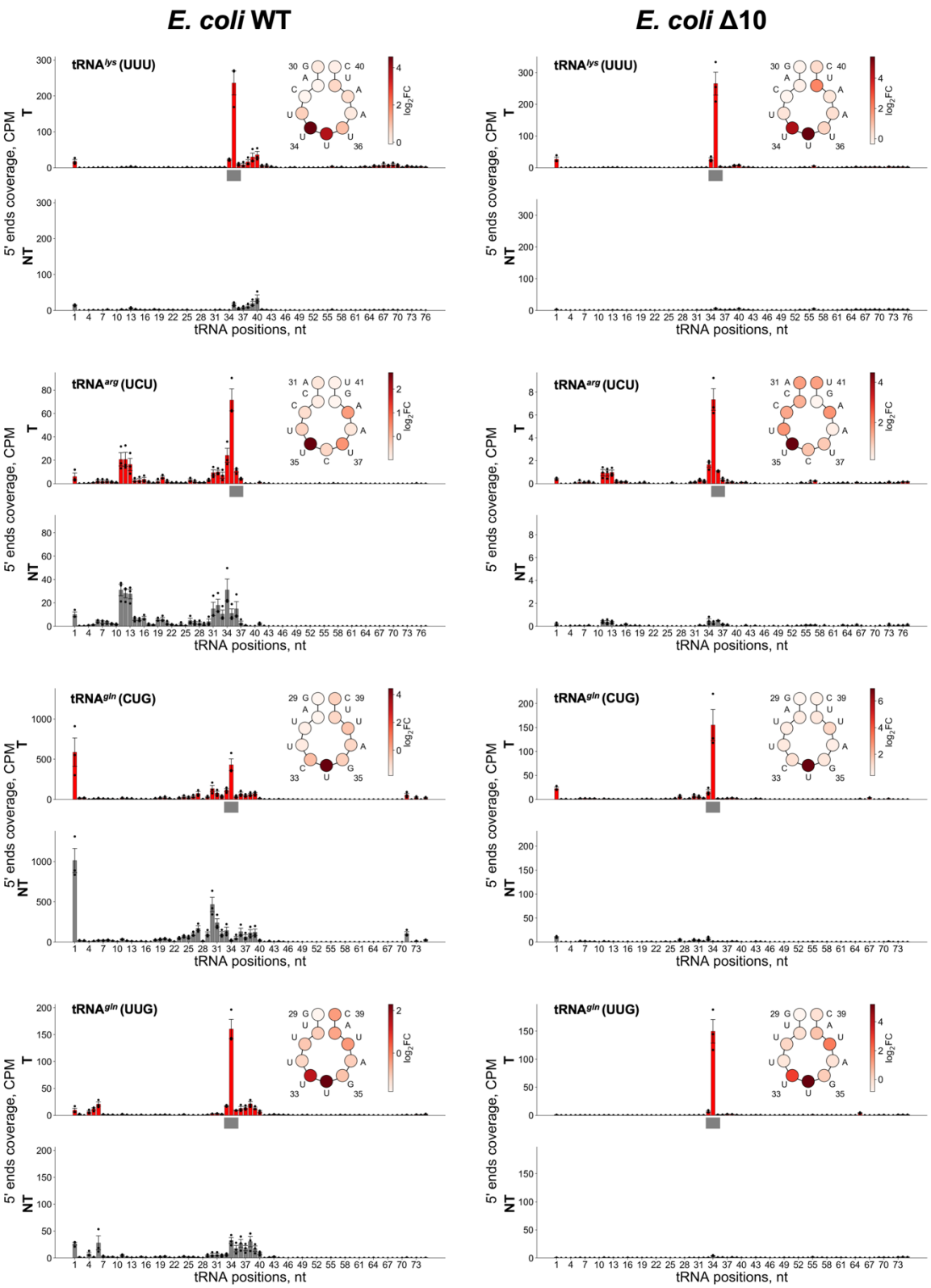

Extended Data Fig. 4. Visualization of cleavage sites in tRNAs in wild type and Δ10 *E. coli* cells. The analysis was performed in the same way as for Fig. 2b: CPM normalized coverage of

5’ ends of transcripts mapped onto tRNA gene in targeting (T, red bars) and nontargeting (NT, grey bars) samples of *E. coli* cells (mean ± s. e. m. from three biological replicates). The horizontal axis depicts the nucleotide position of tRNA. The region corresponding to the anticodon is shown by a grey bar. At the top right part of each panel the scheme of tRNA anticodon loop is depicted; circles correspond to tRNA nucleotides. Each circle is colored according to color scheme where the intensity of color corresponds to values of $\log_2$FC between mean 5’ ends CPMs in targeting and nontargeting samples.

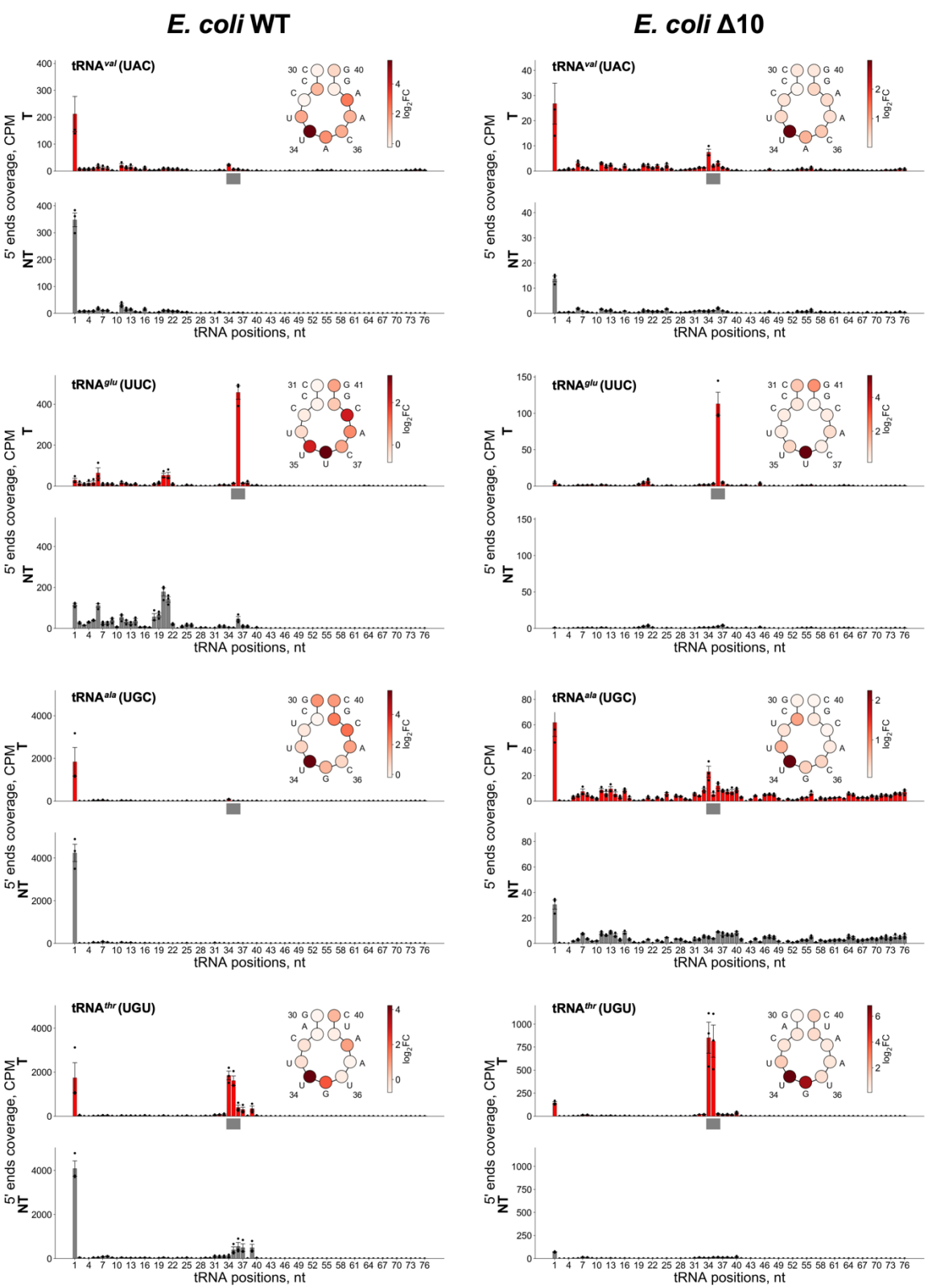

Extended Data Fig. 4 continued.

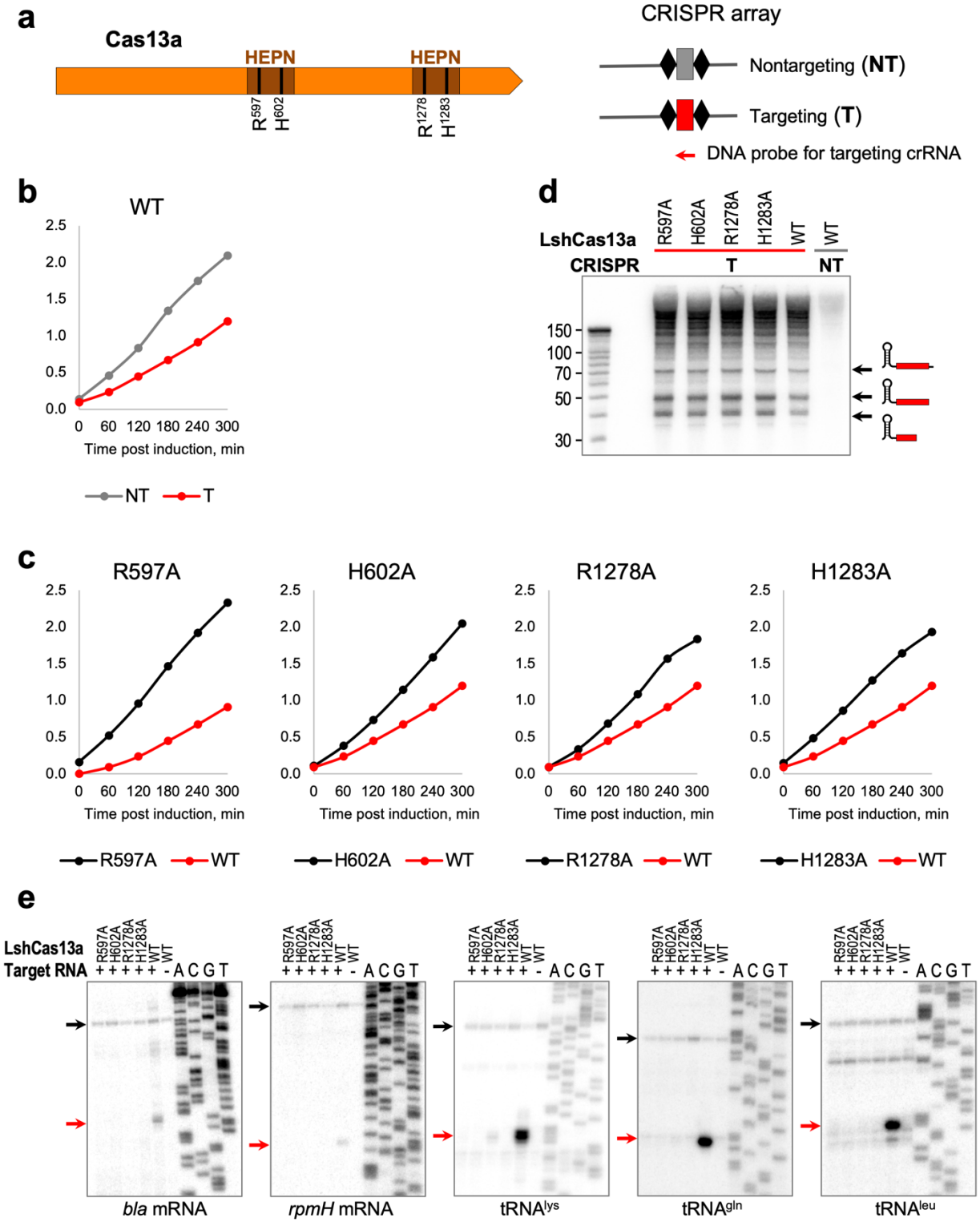

Extended Data Fig. 5. Effect of HEPN catalytic residue mutations on cell growth, crRNA processing, and RNA cleavage in cells expressing target-activated Cas13a.

a, Schematic of the domain organization of LshCas13a protein showing catalytic residues of HEPN domains. CRISPR array structures for cells used in these experiments are shown on the right. **b**, **c**, Single substitution of any of four catalytic residues restores growth in cells expressing mutant Cas13a, crRNA and complementary target RNA, the growth rate is similar to that of nontargeting control cells expressing wild type Cas13. **d**, HEPN mutations do not affect crRNA processing. **e**, HEPN mutations abolish mRNA and tRNA cleavages. All gels are representative of three biological replicates. For gel source data, see Supplementary Fig. 2.

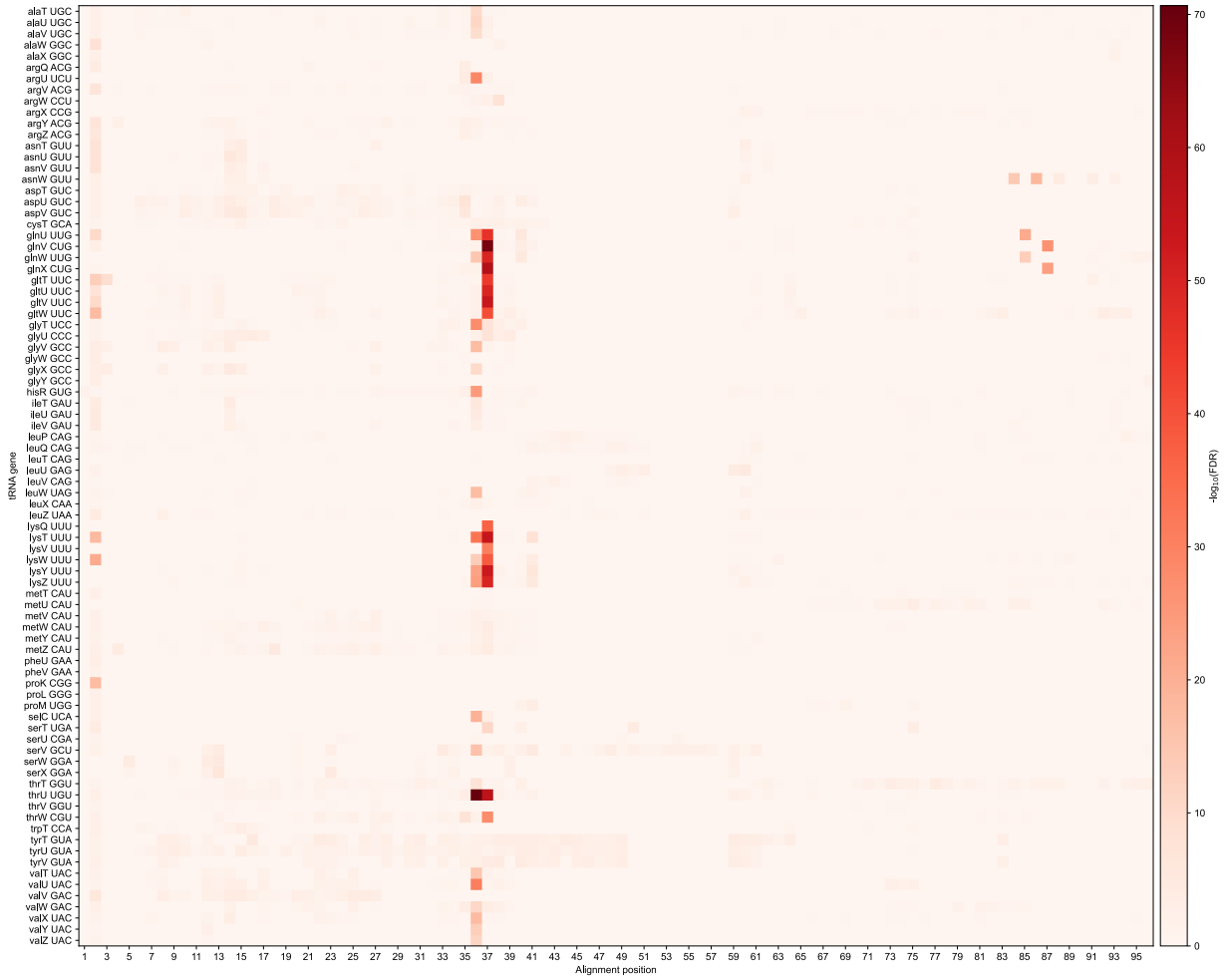

Extended Data Fig. 6. The preference of the cleavage of different tRNAs in Δ10 strain. The nucleotide sequences of tRNA genes were aligned. The horizontal axis depicts the position of the multiple sequence alignment. The vertical axis corresponds to different tRNA genes. The positions of each tRNA in the alignment were assigned with the corresponding -log10(adjusted p-value) that depicts the statistical significance of the cleavage in the given position. The positions corresponding to gaps or the positions excluded from the analysis were assigned with zero values. The resulting table was visualized as the heatmap where the intensity of color depicts the -log10(adjusted p-value).

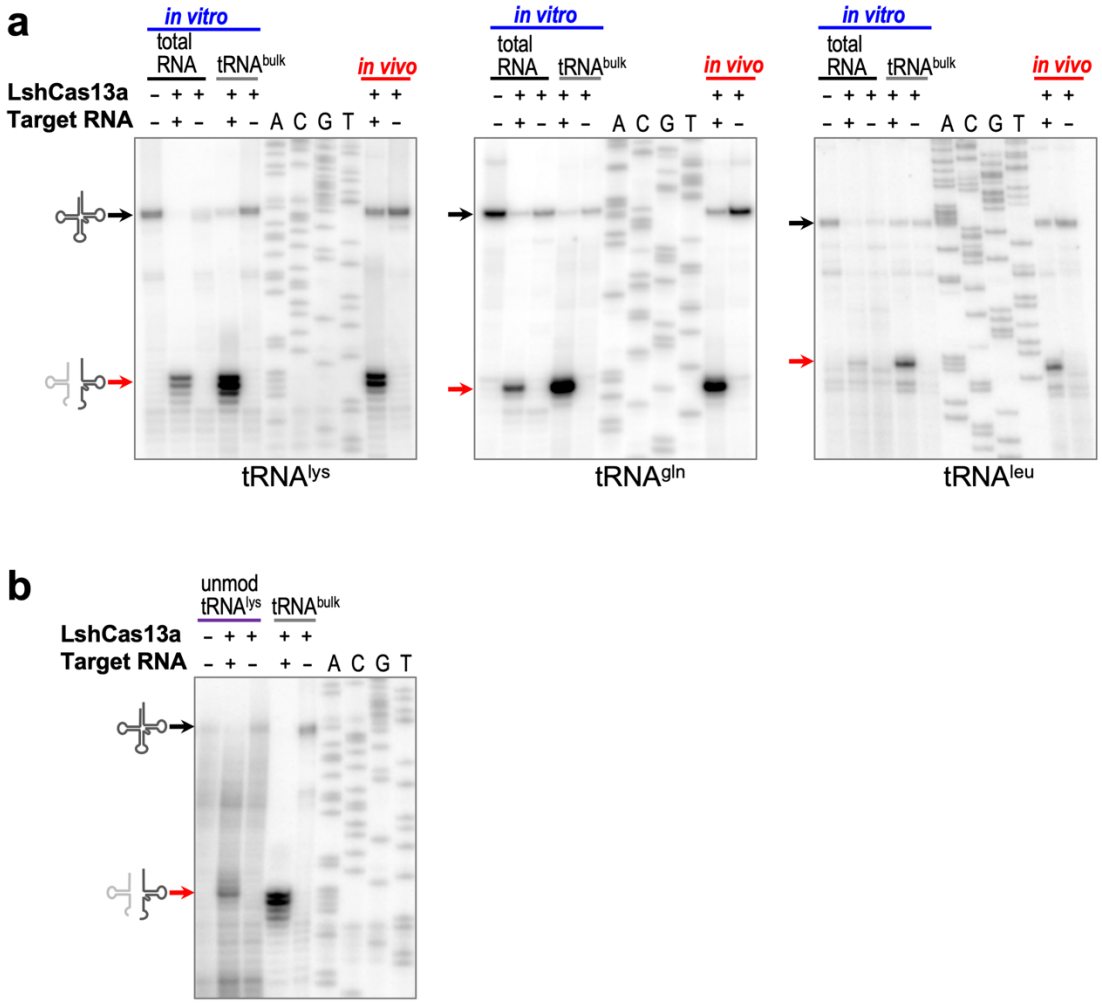

Extended Data Fig. 7. tRNA cleavage *in vitro*. a, Total RNA used as a substrate for cleavage by Cas13a *in vitro*. Primer extension assay revealed that position of cleavage sites at tRNA anticodon loop is unchanged when total *E. coli* RNA or bulk *E. coli* tRNA is used as cleavage substrate *in vitro* and matches those observed *in vivo*. **b**, Cas13a cleaves synthetic $tRNA^{lys}$ at the anticodon loop - nucleoside modifications in tRNA are not required for cleavage. All gel images are representative of three independent experiments. For gel source data, see Supplementary Fig. 2.

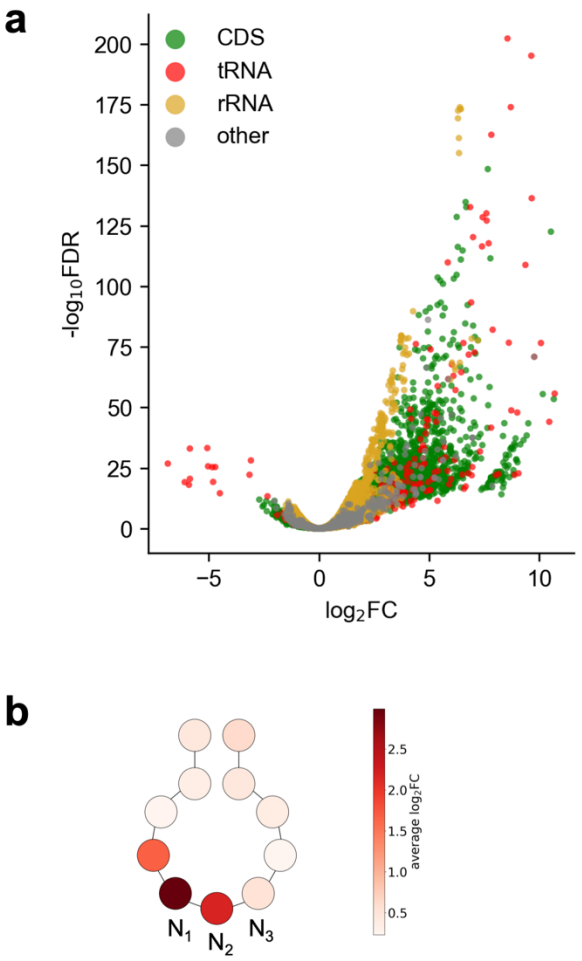

Extended Data Fig. 8. RNA-seq of *in vitro* Cas13a cleavage products.
a, Volcano plot depicting the results of the comparison of 5' transcripts ends counts per nucleotide position of each strand between targeting and nontargeting samples in *in vitro* cleavage experiments with isolated total *E. coli* RNA. The analysis was performed in the same way as for Fig. 3d: likelihood ratio test was used. Each dot corresponds to analyzed nucleotide position. The horizontal axis depicts log_2FC value between targeting and nontargeting samples; the vertical axis depicts adjusted p-value. Dot colors correspond to genomic features where the analyzed nucleotide position is located. **b**, Schematic depiction of tRNA anticodon loop; circles correspond to tRNA nucleotides. Each circle is colored according to color scheme where the intensity of color corresponds to average value of log_2FC between average 5' ends CPMs in targeting and nontargeting samples across all tRNA genes detected in *E. coli* genome.

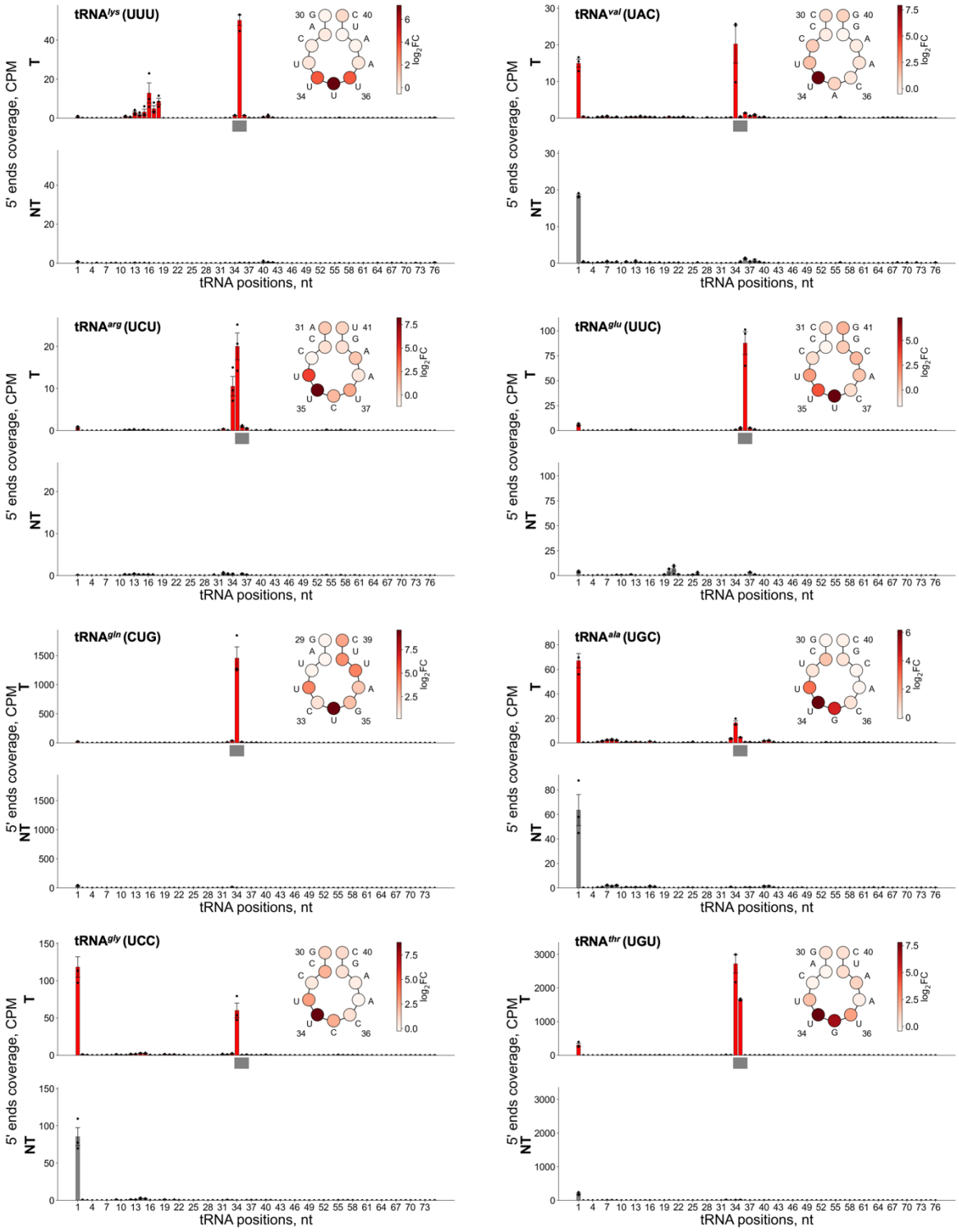

Extended Data Fig. 9. Mapping *in vitro* tRNA cleavage sites. CPM normalized coverage of 5' ends of transcripts mapped onto tRNA gene in targeting (T, red bars) and nontargeting (NT, grey bars) *in vitro* samples (mean ± s. e. m. from three independent experiments). The horizontal axis depicts the nucleotide position of tRNA. The region corresponding to anticodon is shown by a

grey bar. At the top right part of each panel the scheme of tRNA anticodon loop is depicted; circles correspond to tRNA nucleotides. Each circle is colored according to color scheme where the intensity of color corresponds to values of $\log_2$FC between mean 5' ends CPMs in targeting and nontargeting samples.

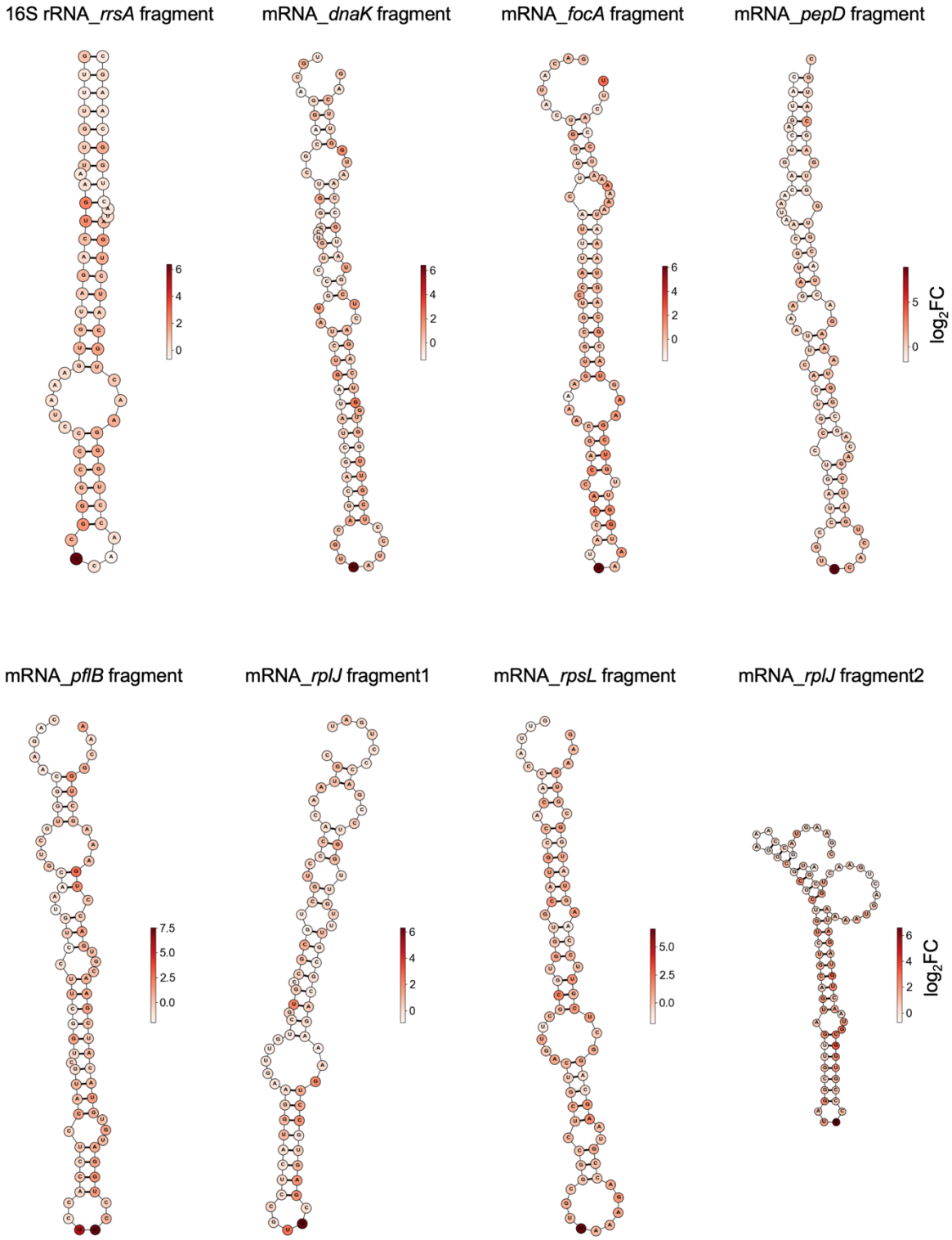

Extended Data Fig. 10. Non-tRNA cleavages by target-activated Cas13a *in vitro*. Mapping of several *in vitro* cleavage sites detected in non-tRNA substrates on the predicted secondary structures of RNA molecules: eighty nucleotides surrounding the analyzed cleavage sites were extracted, and the RNA secondary structures were predicted using RNAfold program (see

Methods). Each circle is colored according to color scheme where the intensity of color corresponds to values of log_2FC between average 5' ends CPMs in targeting and nontargeting samples. Non-tRNA cleavages at uridine residues located at small loops mimic tRNA cleavages at *in vitro* conditions.